

# On the precision of full-spectrum fitting of stellar populations – III. Identifying age spreads

Randa Asa'd<sup>1</sup>,<sup>1,2</sup>★ Paul Goudfrooij<sup>1,2</sup>, A. M. As'ad,<sup>3</sup> H. G. El-Mir,<sup>4</sup> L. Begum,<sup>4</sup> A. Aljasmii<sup>4</sup> and O. Almatroushi<sup>4</sup>

<sup>1</sup>Physics Department, American University of Sharjah, PO Box 26666, Sharjah, UAE

<sup>2</sup>Space Telescope Science Institute, 3700 San Martin Drive, Baltimore, MD 21218, USA

<sup>3</sup>King Abdullah II School for Information Technology, University of Jordan, Amman, Jordan

<sup>4</sup>American University of Sharjah, PO Box 26666, Sharjah, UAE

Accepted 2021 April 1. Received 2021 April 1; in original form 2021 January 25

## ABSTRACT

In this third paper of a series on the precision of obtaining ages of stellar populations using the full-spectrum fitting technique, we examine the precision of this technique in deriving possible age spreads within a star cluster. We test how well an internal age spread can be resolved as a function of cluster age, population, mass fraction, and signal-to-noise ratio (S/N). For this test, the two ages (Age (SSP<sub>1</sub>) and Age (SSP<sub>2</sub>)) are free parameters along with the mass fraction of SSP<sub>1</sub>. We perform the analysis on 118 800 mock star clusters covering all ages in the range  $6.8 < \log(\text{age/yr}) < 10.2$ , with mass fractions from 10 per cent to 90 per cent for two age gaps (0.2 and 0.5 dex). Random noise is added to the model spectra to achieve S/N ratios between 50 and 100 per wavelength pixel. We find that the mean of the derived Age (SSP<sub>1</sub>) generally matches the real Age (SSP<sub>1</sub>) to within 0.1 dex up to ages around  $\log(\text{age/yr}) = 9.5$ . The precision decreases for  $\log(\text{age/yr}) > 9.6$  for any mass fraction or S/N, due to the similarity of SED shapes for those ages. In terms of the recovery of age spreads, we find that the derived age spreads are often larger than the real ones, especially for  $\log(\text{age/yr}) \lesssim 8.0$  and high mass fractions of SSP<sub>1</sub>. Increasing the age gap in the mock clusters improves the derived parameters, but Age (SSP<sub>2</sub>) is still overestimated for the younger ages.

**Key words:** galaxies: star clusters: general.

## 1 INTRODUCTION

In the first paper of this series (Asa'd & Goudfrooij 2020, hereafter Paper I), we investigated the precision of the ages and metallicities of 21 000 mock simple stellar populations (SSPs) determined through full-spectrum fitting in the optical range. We found that for  $S/N \geq 50$ , this technique can yield ages of SSPs to an overall precision of  $\Delta \log(\text{age/yr}) \sim 0.1$  for ages in the ranges  $7.0 \leq \log(\text{age/yr}) \leq 8.3$  and  $8.9 \leq \log(\text{age/yr}) \leq 9.4$ . For the age ranges of  $8.3 \leq \log(\text{age/yr}) \leq 8.9$  and  $\log(\text{age/yr}) \geq 9.5$ , the age uncertainty rises to about  $\pm 0.3$  dex. In the second paper of the series (Goudfrooij & Asa'd 2021, hereafter Paper II) we studied the influence of star cluster mass through stochastic fluctuations of the number of stars near the top of the stellar mass function, which dominate the flux in certain wavelength regimes depending on the age. Studying several wavelength intervals in the  $0.35\text{--}5.0 \mu\text{m}$  range, we found that in general, the spectral shape in the blue optical regime ( $0.35\text{--}0.7 \mu\text{m}$ ) is by far the least impacted by stochastic fluctuations among the wavelength intervals studied. In both previous studies we followed the assumption that star clusters as SSPs, considering all constituent stars to have the same age and metallicity. However, most old globular clusters (GCs) are now known to host abundance variations of several light elements (mainly He, C, N, O, Na, and Al; see Bastian &

Lardo 2018, for details). This phenomenon is often referred to as Multiple Stellar Populations (MSPs). Interestingly, MSPs have not yet been identified in clusters younger than  $\sim 2$  Gyr (see Martocchia et al. 2018; Asa'd et al. 2020; Cabrera-Ziri et al. 2020; Li et al. 2020). However, if young massive clusters (YMCs) are the young analogues of GCs, one might expect to find MSPs in YMCs. The role that age plays in the MSP phenomenon has been difficult to constrain (e.g. Cabrera-Ziri et al. 2020). Additionally, several studies, based on accurate *Hubble Space Telescope* (HST) photometry and *Gaia*, have revealed that the colour–magnitude diagram (CMD) of stellar clusters younger than  $\sim 2$  Gyr exhibits an extended main-sequence turn-off (eMSTO) which is not due to photometric errors, field-star contamination, differential reddening, or non-interacting binaries (e.g. Bertelli et al. 2003; Mackey & Broby Nielsen 2007; Goudfrooij et al. 2009; Milone et al. 2009; Cordoni et al. 2018, and references therein). These findings have challenged the traditional picture that the CMDs of star clusters are well described by SSPs, and have triggered huge efforts to understand eMSTOs. The eMSTO phenomenon was initially proposed to be due to multiple stellar formation events, challenging the conventional belief that star clusters are groups of coeval stars. However, alternative scenarios to explain this phenomenon were soon proposed as well. The effects of stellar rotation, first proposed by Bastian & de Mink (2009), are currently one of the most widely accepted scenarios (see e.g. Dupree et al. 2017; Bastian et al. 2018; Marino et al. 2018; Sun et al. 2019). However, it is still argued that age spreads may be present in clusters

\* E-mail: [raasad@aus.edu](mailto:raasad@aus.edu)

(see Goudfrooij, Girardi & Correnti 2017; Goudfrooij et al. 2018; Costa et al. 2019; Gossage et al. 2019).

Integrated-light spectra of star clusters have proven to be accurate tools for studying extragalactic clusters for which spatially resolved data are not available (Ahumada et al. 2002; Puzia et al. 2005; Puzia, Kissler-Patig & Goudfrooij 2006; Santos et al. 2006; Palma et al. 2008; Cid Fernandes & Gonzalez Delgado 2010; Talavera et al. 2010; Asa'd, Hanson & Ahumada 2013; Asa'd 2014; Chilingarian & Asa'd 2018). In this work, we aim to address the question: To what extent can integrated-light spectra be used to identify age spreads at different ages?

## 2 MOCK STAR CLUSTERS

We create a sample of mock star cluster spectra following the results of Paper I: (A) We used the wavelength range 3700–5000 Å which we showed to be optimal for deriving accurate ages from integrated-light spectra using the full-spectrum fitting method. (B) our sample has  $S/N > 50$ ; (C) the smallest age difference (gap) used to create the age combinations is 0.2 dex. We use the flexible stellar population synthesis (FSPS) code (Conroy, Gunn & White 2009; Conroy & Gunn 2010) operated through the Python package python-FSPS (Foreman-Mackey, Sick & Johnson 2014) to create integrated-light spectra of SSPs for the wavelength range 3700–5000 Å with Kroupa (2001) IMF and fixed metallicity  $[Z/H] = -0.4$  for the age range  $7.0 < \log \text{age} < 10.2$  in steps of 0.1 dex using MIST isochrones (Choi, Conroy & Byler 2017) and the MILES spectral library (Sánchez-Blázquez et al. 2006; Vazdekis et al. 2010, 2016), which has a spectral resolution of 2.5 Å (Falcón-Barroso et al. 2011). We use the default settings of python-FSPS (similar to Paper I and Paper II), including the absence of nebular emission for the youngest ages, and a zero fraction of blue horizontal branch stars at old ages. We then combine two SSPs, in order to explore if our method can derive age spreads where two SSPs are present, according to the equation:

$$f \text{ SSP}_1 + (1 - f) \text{ SSP}_2, \quad (1)$$

where  $f$  is the fractional contribution of  $\text{SSP}_1$  by mass, running from 0 to 1 in steps of 0.1,  $\text{SSP}_1$  is the SSP of an arbitrary age, and  $\text{SSP}_2$  is the additional SSP. We start with a sample that has an age gap of 0.2 dex and can be described by the following equation:

$$\log(\text{age}(\text{SSP}_2)) = \log(\text{age}(\text{SSP}_1)) + 0.2. \quad (2)$$

Finally, we add 30 different realizations of random noise, corresponding to  $S/N$  values between 50 and 100 (in steps of 10) for each combination, thus producing a grand total of 59 400 mock clusters.

## 3 FITTING SINGLE AGE

### 3.1 Method

We first assume that the sample of mock clusters consists of only one SSP, and use the full-spectrum fitting program ASAD<sub>2</sub> (for a full description, see Asa'd et al. 2013; Asa'd 2014; Asa'd, Vazdekis & Zeinelabdin 2016) to obtain the best-fitting age using the following equation:

$$\sum_{\lambda=\lambda_{\text{initial}}}^{\lambda_{\text{final}}} \frac{[(OF)_{\lambda} - (MF)_{\lambda}]^2}{(OF)_{\lambda_{\text{norm}}}}, \quad (3)$$

where OF is the mock cluster flux, MF is the SSP model flux, and  $\lambda_{\text{norm}}$  is the wavelength at which the model and the mock cluster spectra are normalized.

## 3.2 Results

When  $f = 0$  in equation (1), the mass fraction of  $\text{SSP}_1 = 0$ , the spectrum is a single SSP (100 per cent contribution from  $\text{SSP}_2$ ). In this case the correct age is always correctly derived for all  $S/N$ . The results obtained for  $0 < f < 1$  are shown in Fig. 1, where we plot the mean of the derived single age with the uncertainty (calculated as the standard deviation) for the 30 realizations of each  $S/N$  and mass fraction  $f$  versus the input age of  $\text{SSP}_2$  in equation (1).

The figure shows that as the mass fraction of  $\text{SSP}_1$  increases, the full-spectrum fitting technique increasingly favours the average age values [i.e.  $(\text{SSP}_1 + \text{SSP}_2)/2$ ]. Once  $f > 60$  per cent, where  $\text{SSP}_1$  dominates, the full-spectrum fitting technique increasingly derives the age of  $\text{SSP}_1$  correctly. For all ages and mass fraction values, there is no significant dependence on the  $S/N$  value in the range tested.

## 4 FITTING TWO AGES

### 4.1 Method

We create the two-age model grid, using equation (1), for all possible combinations of  $\text{SSP}_1$  and  $\text{SSP}_2$  with an age gap of 0.2 dex between the two SSPs, and attempt to recover  $\text{Age}(\text{SSP}_1)$ ,  $\text{Age}(\text{SSP}_2)$ , and  $f$  using the full-spectrum fitting technique. The results obtained are arranged so that  $\text{Age}(\text{SSP}_1)$  is always less than  $\text{Age}(\text{SSP}_2)$ . We tested the technique first on the trivial case where no noise was added to the combined spectra and the input parameters were perfectly recovered.

### 4.2 Results

#### 4.2.1 Derived $\text{Age}(\text{SSP}_1)$ and $\text{Age}(\text{SSP}_2)$

In order to assess to what extent integrated-light spectra can be used to identify age spreads at different ages, we first examine the mean derived age for each input SSP age in the combination. Fig. 2 shows the mean of the derived ages with the uncertainty (calculated as the standard deviation) for the 30 realizations of each  $S/N$  and mass fraction  $f$  versus the input age. The top set of panels shows the results of  $\text{Age}(\text{SSP}_1)$  and the bottom set of panels shows the results of  $\text{Age}(\text{SSP}_2)$ . Overall, the mean of the derived  $\text{Age}(\text{SSP}_1)$  matches the real  $\text{Age}(\text{SSP}_1)$  up to ages around  $\log(\text{age/yr}) = 9.5$ . The precision decreases for  $\log(\text{age/yr}) > 9.6$  for any mass fraction or  $S/N$ . The shape of the SED does not change much beyond  $\log(\text{age/yr}) = 9.6$ , causing age estimates to be relatively imprecise for those ages (see Paper I and Paper II for more discussion on this).

The uncertainty associated with the mean of the derived  $\text{Age}(\text{SSP}_2)$  (see lower set of panels of Fig. 2) is much higher than that of  $\text{Age}(\text{SSP}_1)$ , especially for young ages. To shed more light on the cause of this result, we list the results of the 30 realizations with  $S/N = 100$  obtained for the input combination of 80 per cent of  $\log(\text{Age}(\text{SSP}_1)) = 7.0$  with 20 per cent of  $\log(\text{Age}(\text{SSP}_2)) = 7.2$ , in Table 1. The list shows that the full-spectrum fitting technique tends to derive combinations of a young age that is close to the real age along with an older age, with the latter age encompassing several orders of magnitude from one mock cluster to another. This is found to be generally the case for young ages ( $\log(\text{age/yr}) < 8.0$ ) and is explained by the fact that SEDs for  $\log(\text{age/yr})$  in the range 7.0–7.5 are very similar to one another, and they produce significantly more flux than older populations (especially in the blue; see e.g. Paper I and Paper II). Hence, the derived two-SSP combination includes one young SSP that is close to the real age, with an older SSP with

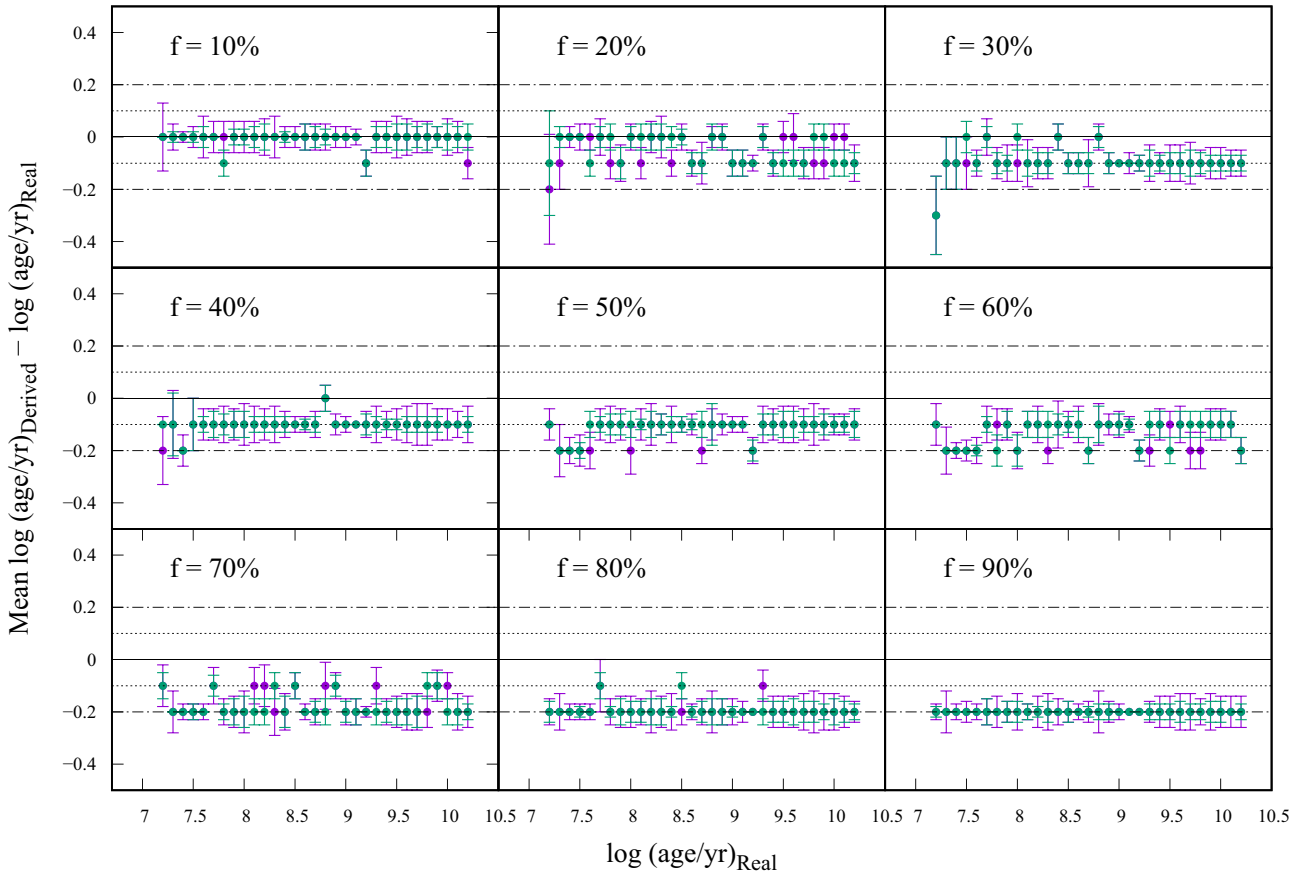


**Figure 1.** The mean derived single age and the uncertainty (calculated as the standard deviation) for the 30 realization of each set versus real age. The green dots represent results for  $S/N = 100$  and the purple dots represent the results for  $S/N = 50$ . The continuous middle line is the  $y = 0$  line, the dotted lines are  $y = \pm 0.1$ , and the dashed lines are  $y = \pm 0.2$ .

almost *any* other age, since the latter does not produce a significant percentage of the flux.

To illustrate this further, a closer look at the mock cluster for which the derived parameters are 30 per cent of  $\text{Age}(\text{SSP}_1) = 7.0$  with 70 per cent  $\text{Age}(\text{SSP}_2) = 9.1$  reveals that the  $\chi^2$  value of this combination is 0.11212. Fig. 3 shows a heat map with all the combinations of  $\text{Age}(\text{SSP}_2)$  and mass fraction that have  $\chi^2$  values between 0.1 and 0.2. The white star shows the coordinates of the combination with the minimum  $\chi^2$  value. The dark blue regions represent the  $\chi^2$  values between 0.100 and 0.111. This shows that combinations of  $\text{Age}(\text{SSP}_1) = 7.0$  with  $\text{Age}(\text{SSP}_2) = 7.7$  to 7.9 and 8.9 to 9.4 are very close to the correct combination (80 per cent of  $\text{Age}(\text{SSP}_1) = 7.0$  with 20 per cent  $\text{Age}(\text{SSP}_2) = 7.2$ ). This explains the results obtained in the lower panel of Fig. 2 where the mean of the derived  $\text{Age}(\text{SSP}_2)$  is overestimated for young ages.

Fig. 4 shows the ‘success rate’ – defined as the number of times the derived parameter matches the input parameter within  $\pm 0.1$  dex – as a function of input age. The success rate of  $\text{SSP}_1$  increases as the input mass fraction  $f$  of this SSP increases. The success rate also depends on the input age. It peaks for  $\log(\text{age}/\text{yr}) \lesssim 7.5$  and around 9.0 (the latter corresponding to RGB phase transition) and it drops around 8.6 and for  $> 9.2$  for almost all mass fractions. In Paper I, we showed that the number of correctly derived ages drop significantly in these age ranges that correspond to the asymptotic giant branch (AGB) phase transition in stellar evolution, and the red giant branch (RGB) phase transition. The age range  $> 9.2$  is the worst in terms of success rate, because SEDs in this age range are very similar to

one another. Identifying small age spreads of two populations that do not fall around a fast evolutionary transition is not trivial. The success rate of  $\text{SSP}_2$  decreases as the input mass fraction  $f$  of  $\text{SSP}_1$  increases, as expected. The success rate peaks at ages very slightly younger than the ones at which it peaks for  $\text{SSP}_1$  in addition to  $\log(\text{age}/\text{yr}) = 10$  for  $f$  from 10 per cent to 40 per cent. It is worth noting that this rise towards the oldest ages is meaningless, since we used  $\Delta\text{SSP} = 0.2$ , so that all the simulations with  $\log(\text{age}(\text{SSP}_1)) > 9.7$  or so can only have  $\log(\text{age}(\text{SSP}_2))$  higher than that, thus boosting their success numbers.

#### 4.2.2 Age spread

Fig. 5 shows the results obtained for the age spread, defined as  $\log(\text{Age}(\text{SSP}_2)) - \log(\text{Age}(\text{SSP}_1))$ . The top panel shows the mean of the ‘(derived – input) age spread’ as a function of the input age. The derived average age spreads are larger than the real ones, and the scatter around the mean values is significant, especially for mean  $\log(\text{age}/\text{yr}) \lesssim 8.5$ . The lower panel shows that the overall success rate for the derived age spread is typically of order 20 per cent, without a strong dependence on input age or mass fraction.

## 5 INCREASING THE AGE GAP

In order to investigate the role of the size of the age gap on the derived parameters, we create a new set of 59 400 mock cluster spectra with

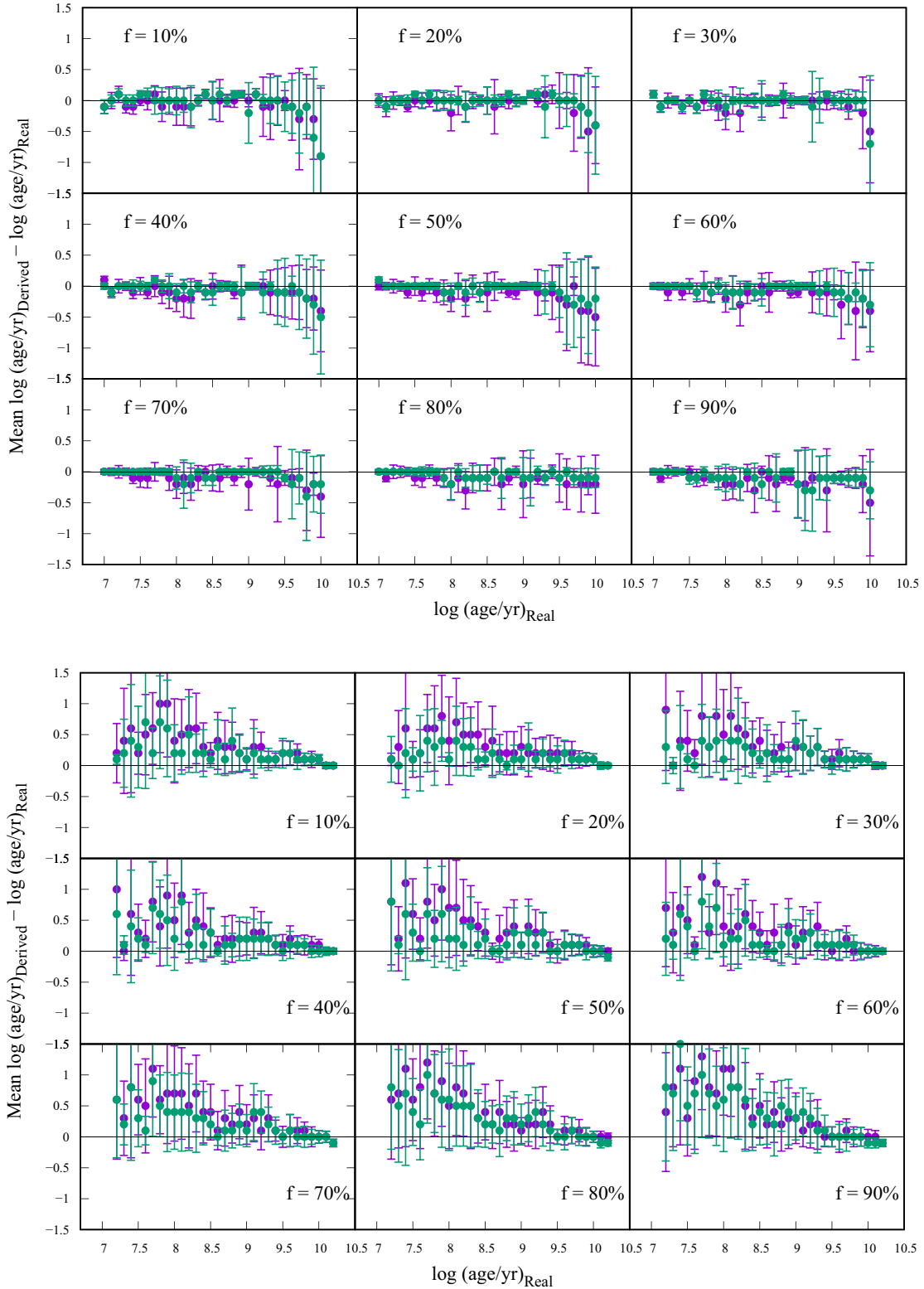


**Figure 2.** The mean of the derived age versus the input age. The top panel shows the results of Age(SSP<sub>1</sub>) and the bottom panel shows the results of Age(SSP<sub>2</sub>). The green dots represent results for  $S/N = 100$  and the purple dots represent the results for  $S/N = 50$ .

larger age step:

$$\log(\text{age}(\text{SSP}_2)) = \log(\text{age}(\text{SSP}_1)) + 0.5 \quad (4)$$

and repeat the analysis aiming to derive Age(SSP<sub>1</sub>), Age(SSP<sub>2</sub>), and  $f$  from the full-spectrum fitting technique. Fig. 6 shows that the mean of both Age(SSP<sub>1</sub>) and Age(SSP<sub>2</sub>) is closer to the real values for mock clusters with Age(SSP<sub>2</sub>) – Age(SSP<sub>1</sub>) = 0.5 dex. Despite the

**Table 1.** Derived results for the input combination of 80 per cent Age(SSP<sub>1</sub>) = 7.0 with 20 per cent Age(SSP<sub>2</sub>) = 7.2.

Age <sub>1</sub>	<i>f</i>	Age <sub>2</sub>	Age <sub>1</sub>	<i>f</i>	Age <sub>2</sub>	Age <sub>1</sub>	<i>f</i>	Age <sub>2</sub>
6.8	10 per cent	7.0	7.0	80 per cent	7.3	7.0	70 per cent	7.8
7.0	40 per cent	7.1	7.0	80 per cent	7.3	7.0	40 per cent	8.9
7.0	40 per cent	7.1	7.0	70 per cent	7.3	7.0	40 per cent	9.0
7.0	30 per cent	7.1	7.0	60 per cent	7.3	7.0	30 per cent	9.1
7.0	80 per cent	7.2	7.0	70 per cent	7.3	7.0	20 per cent	9.4
7.0	80 per cent	7.2	7.0	70 per cent	7.3	7.0	20 per cent	9.4
7.0	80 per cent	7.2	7.0	70 per cent	7.6	7.0	20 per cent	9.4
7.0	80 per cent	7.2	7.0	70 per cent	7.7	7.0	10 per cent	9.8
7.0	80 per cent	7.2	7.0	70 per cent	7.7	7.0	10 per cent	9.8
7.0	80 per cent	7.3	7.0	70 per cent	7.7	7.0	10 per cent	9.8

increase in the age gap, our results show that the full-spectrum fitting technique still overestimates Age(SSP<sub>2</sub>) consistently for Age(SSP<sub>2</sub>) < 8.5. Fig. 7 shows the success rate as a function of input age. For Age(SSP<sub>1</sub>), the success rate depends on both the mass fraction *f* and the input age. For mass fraction *f* = 10, when SSP<sub>2</sub> is dominating, the success rate is very poor, however for mass fraction *f* > 30 the success rate increases significantly, with drops seen around log (age/yr) = 8.0 and log (age/yr) > 9.4 due to the similarity of the SEDs in the age ranges where the success numbers are low. When comparing the success rate of both Age(SSP<sub>1</sub>) and Age(SSP<sub>2</sub>) for mock clusters that have age gap = 0.5 dex with that of mock clusters that have age gap = 0.2 dex, we notice that the numbers are higher for age gap = 0.2. The reason is that by definition the success rate is the number of times the derived age matches the real age to within ± 0.1 dex, hence smaller age gaps are closer to this precision limit. The mean of the derived age spread for an input age gap of 0.5 is shown in Fig. 8. The results are better than for an age gap of 0.2, although the recovery rate of success to within 0.1 dex (lower panel) did not change significantly.

## 6 RECOVERY OF MASS FRACTION

Now we discuss the precision in recovering the mass fraction for the two cases analysed in the previous sections (i.e. Δ log (age/yr) = 0.2 and 0.5). Fig. 9 shows the mean of the derived mass fraction as a function of the input age. Overall the derived mass fraction is

overestimated for low mass fractions and underestimated for high mass fractions. The best results are achieved when the mass fraction is around 50 per cent.

## 7 SUMMARY

We investigate the accuracy and precision of recovering possible age spreads within a star cluster using the full-spectrum fitting method. We analyse optical spectra of 118 800 mock star clusters with mass fractions from 10 per cent to 90 per cent for two age gaps (0.2 and 0.5 dex) in the age range 6.8 < log (age/yr) < 10.2. Random noise is added to the model spectra to achieve S/N ratios between 50 and 100 per wavelength pixel. We summarize our results in the following points:

(A) The results obtained using the full-spectrum fitting method to derive the age of a star cluster that has an age spread of 0.2 dex depend on the age and the mass fraction of each of the combined SSPs. If one SSP is dominating the spectrum, the full-spectrum fitting technique correctly predicts the age of the dominating SSP. When the contribution of the two SSPs is roughly equal, the full-spectrum fitting technique correctly predicts the average age value of the two SSPs [i.e. ((SSP<sub>1</sub>)+(SSP<sub>2</sub>))/2]. For all ages and mass fraction values, there is no significant dependence on the S/N value in the range 50–100.

(B) When using the full-spectrum fitting method to derive combinations of ages with different mass fractions, the mean of the derived Age(SSP<sub>1</sub>) matches the real Age(SSP<sub>1</sub>) to within 0.1 dex up to ages around log (age/yr) = 9.5. The precision decreases for log (age/yr) > 9.6 for all mass fractions or S/N values. This is because SSP SEDs are very similar in that age range, which makes it difficult to identify their correct age.

(C) For young ages (log (age/yr) ≲ 8.0) the full-spectrum fitting technique tends to derive combinations of a young age with a significantly older age. This is because young populations (log (age/yr) ≲ 7.0) produce significantly more flux than old populations, hence different combinations of young populations with old populations will have very similar χ<sup>2</sup> values, causing the large uncertainty for the mean of the derived Age(SSP<sub>1</sub>) and Age(SSP<sub>2</sub>) as shown in Fig. 2.

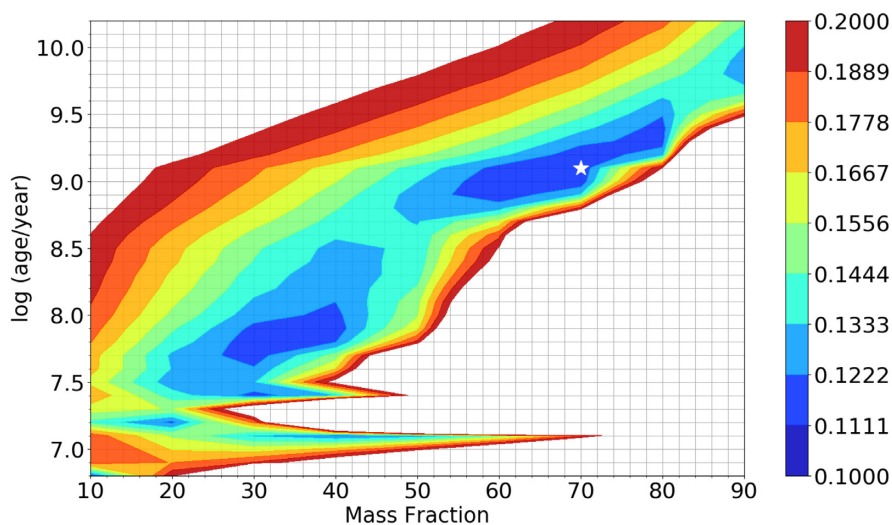


**Figure 3.** The heat map for Age(SSP<sub>2</sub>) of the mock cluster where the derived parameters are Age(SSP<sub>1</sub>) = 7.0 with 70 per cent Age(SSP<sub>2</sub>) = 9.1 in Table 1. The white star shows the coordinates of the combination with the minimum χ<sup>2</sup> value.

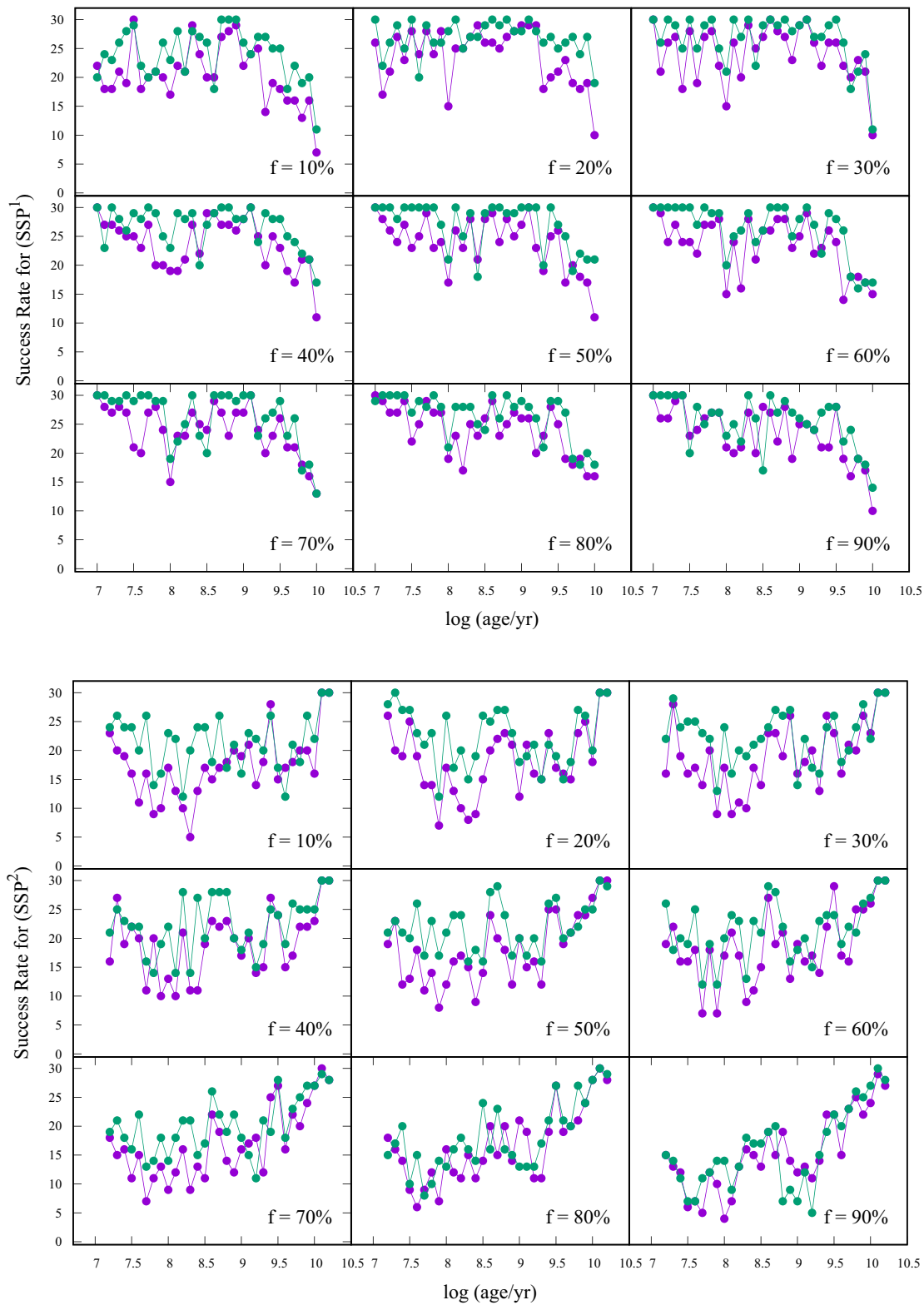


**Figure 4.** The number of successfully recovered ages (i.e. the number of times the derived age matches the real age within  $\pm 0.1$  dex) as a function of real age. The top panel shows the results of Age(SSP<sub>1</sub>) and the bottom panel shows the results of Age(SSP<sub>2</sub>).

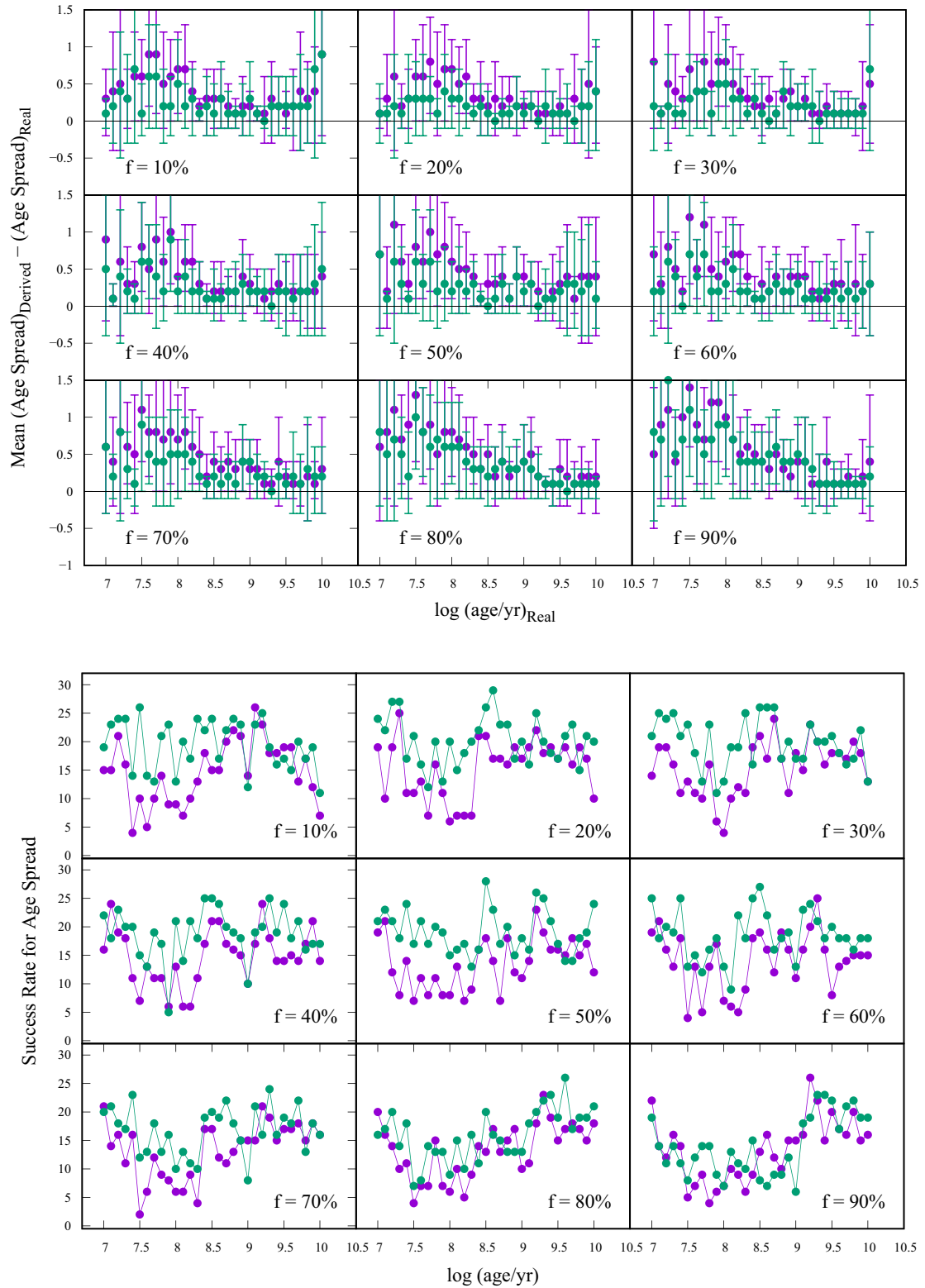


**Figure 5.** The results for the derived age spread, defined as  $\log(\text{Age}(\text{SSP}_2)) - \log(\text{Age}(\text{SSP}_1))$ . The top panel shows the mean of the ‘derived – input’ age spread as a function of the input age and the lower panel shows the recovery success rate as a function of input age.

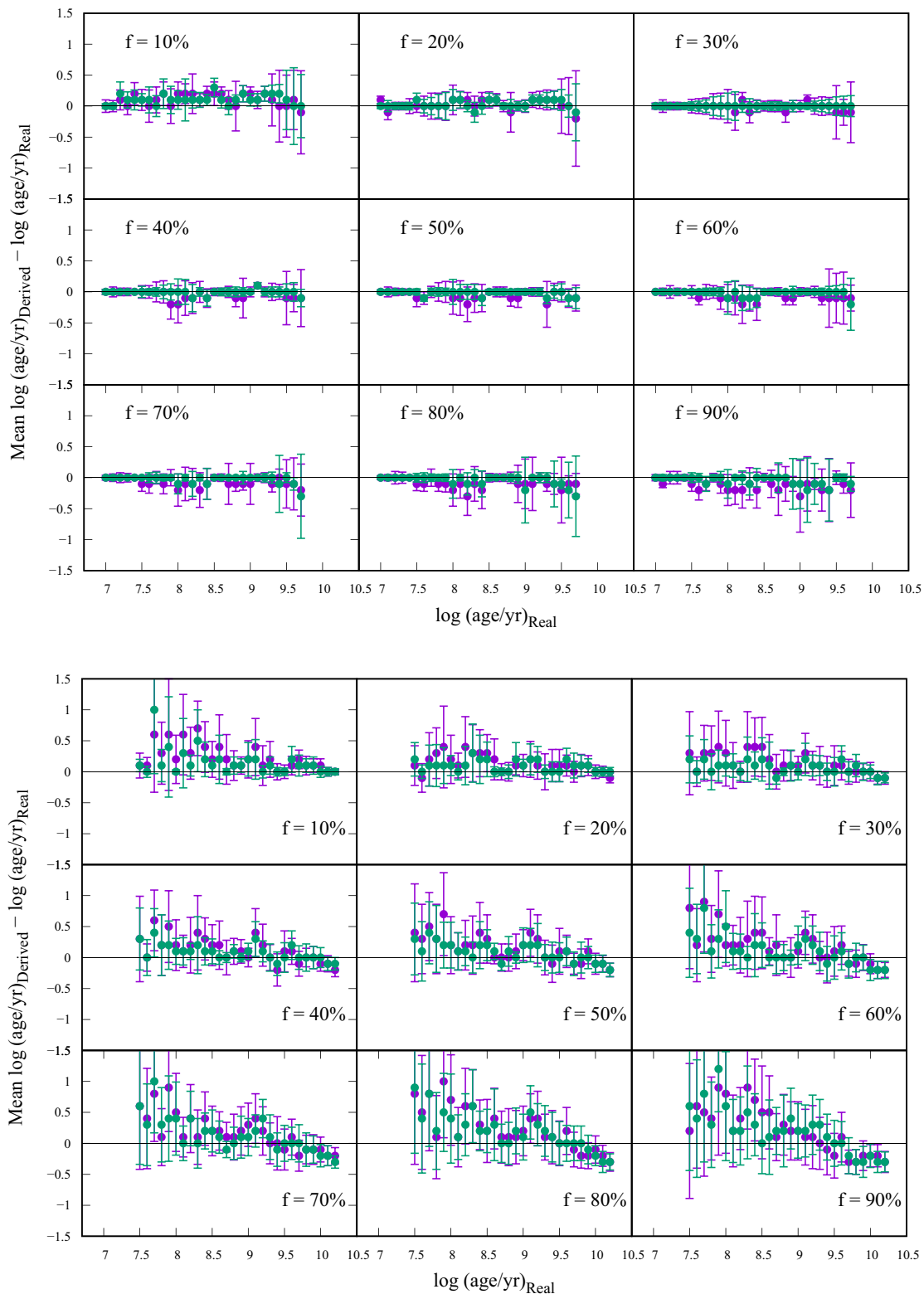


**Figure 6.** The mean of the derived age versus the input age for mock clusters with  $\text{Age}(\text{SSP}_2) - \text{Age}(\text{SSP}_1) = 0.5$ . The top panel shows the results of  $\text{Age}(\text{SSP}_1)$  and the bottom panel shows the results of  $\text{Age}(\text{SSP}_2)$ . The green dots represent results for  $S/N = 100$  and the purple dots represent the results for  $S/N = 50$ .

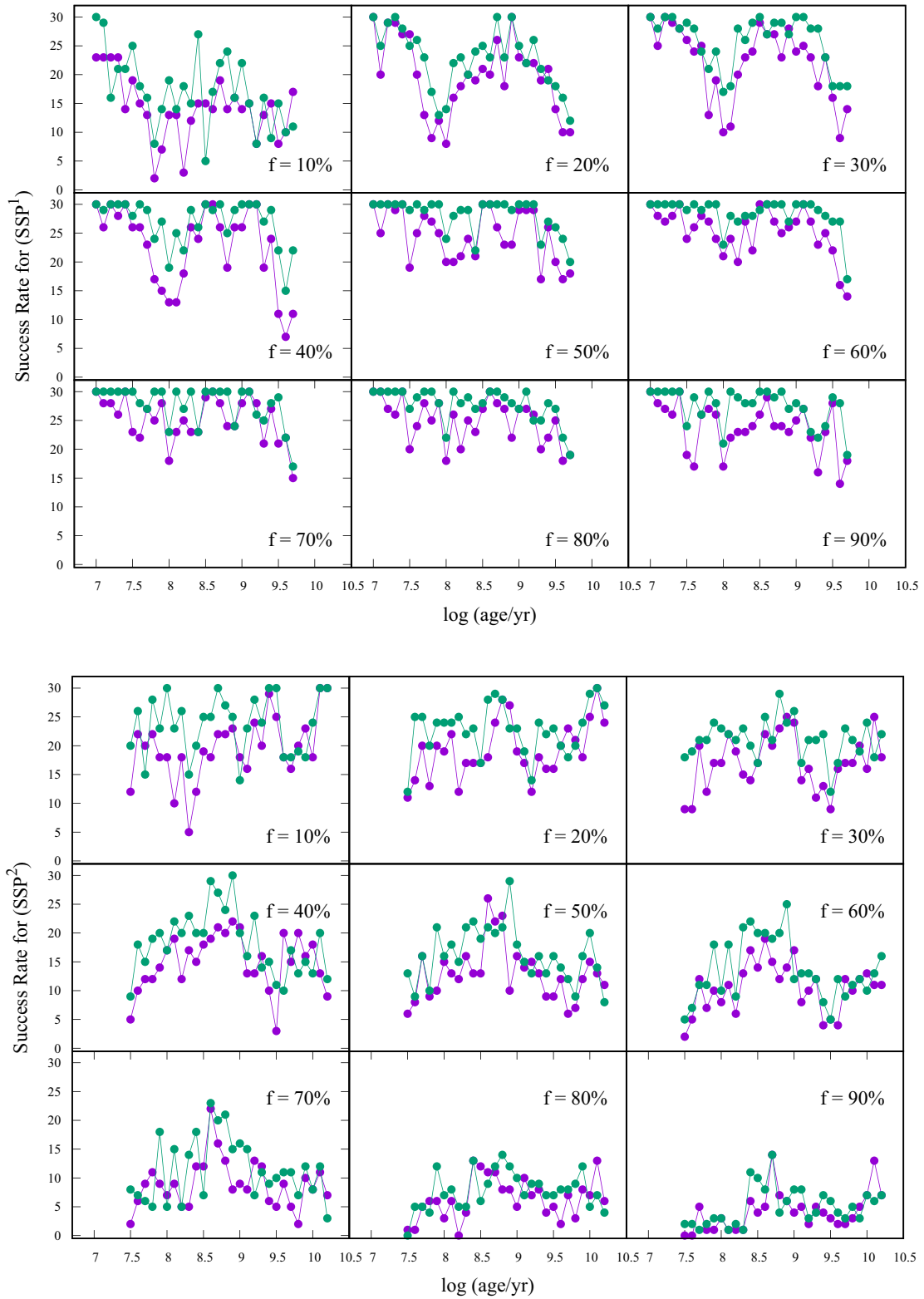


**Figure 7.** The number of successfully recovered ages (i.e. the number of times the derived age matches the real age  $\pm 0.1$  dex) as a function of real age for mock clusters with  $\text{Age}(\text{SSP}_2) - \text{Age}(\text{SSP}_1) = 0.5$ . The top panel shows the results of  $\text{Age}(\text{SSP}_1)$  and the bottom panel shows the results of  $\text{Age}(\text{SSP}_2)$ . The green dots represent results for  $S/N = 100$  and the purple dots represent the results for  $S/N = 50$ .

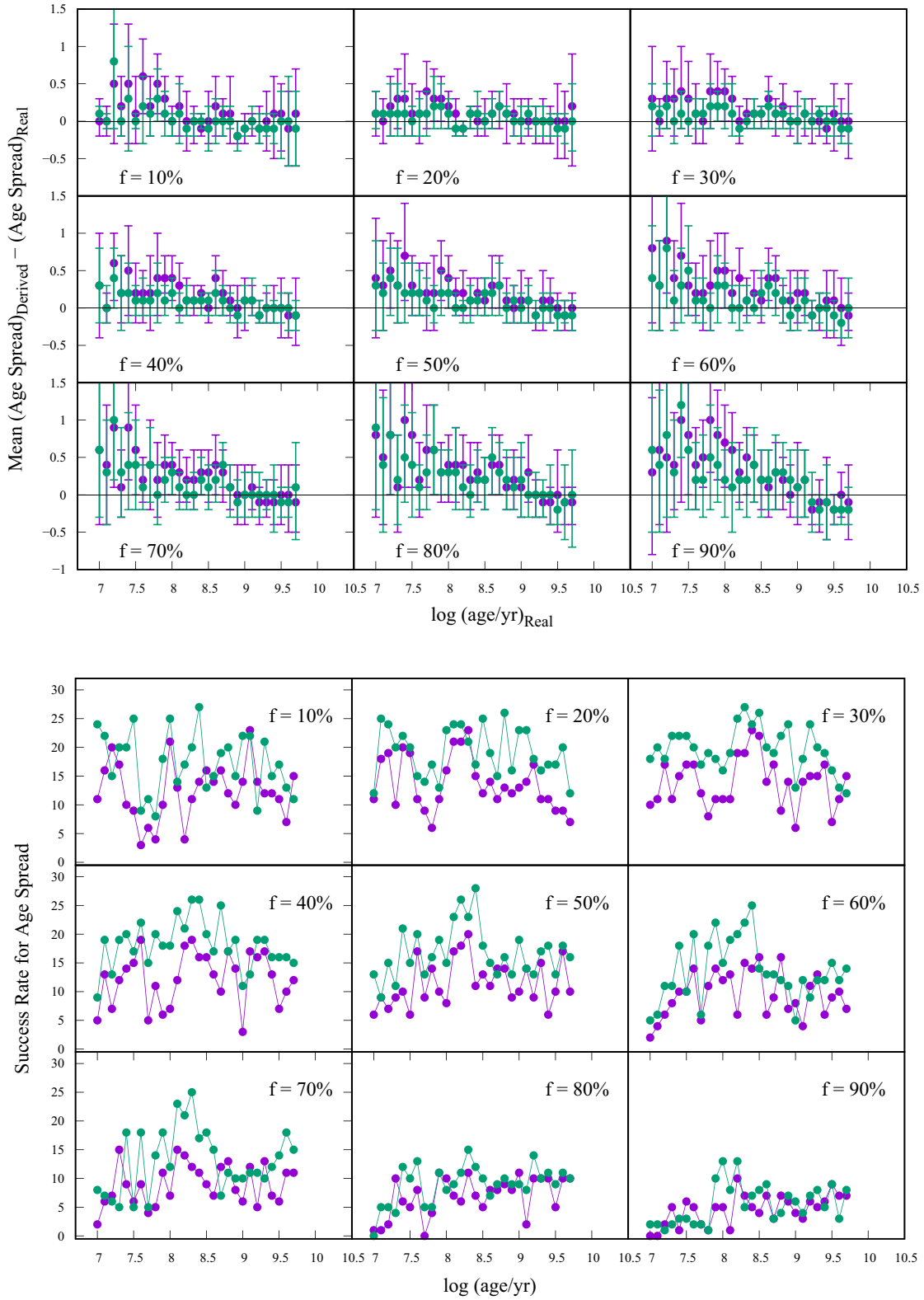


**Figure 8.** The same as Fig. 5, but now for input  $\Delta(\log(\text{age/yr})) = 0.5$ .

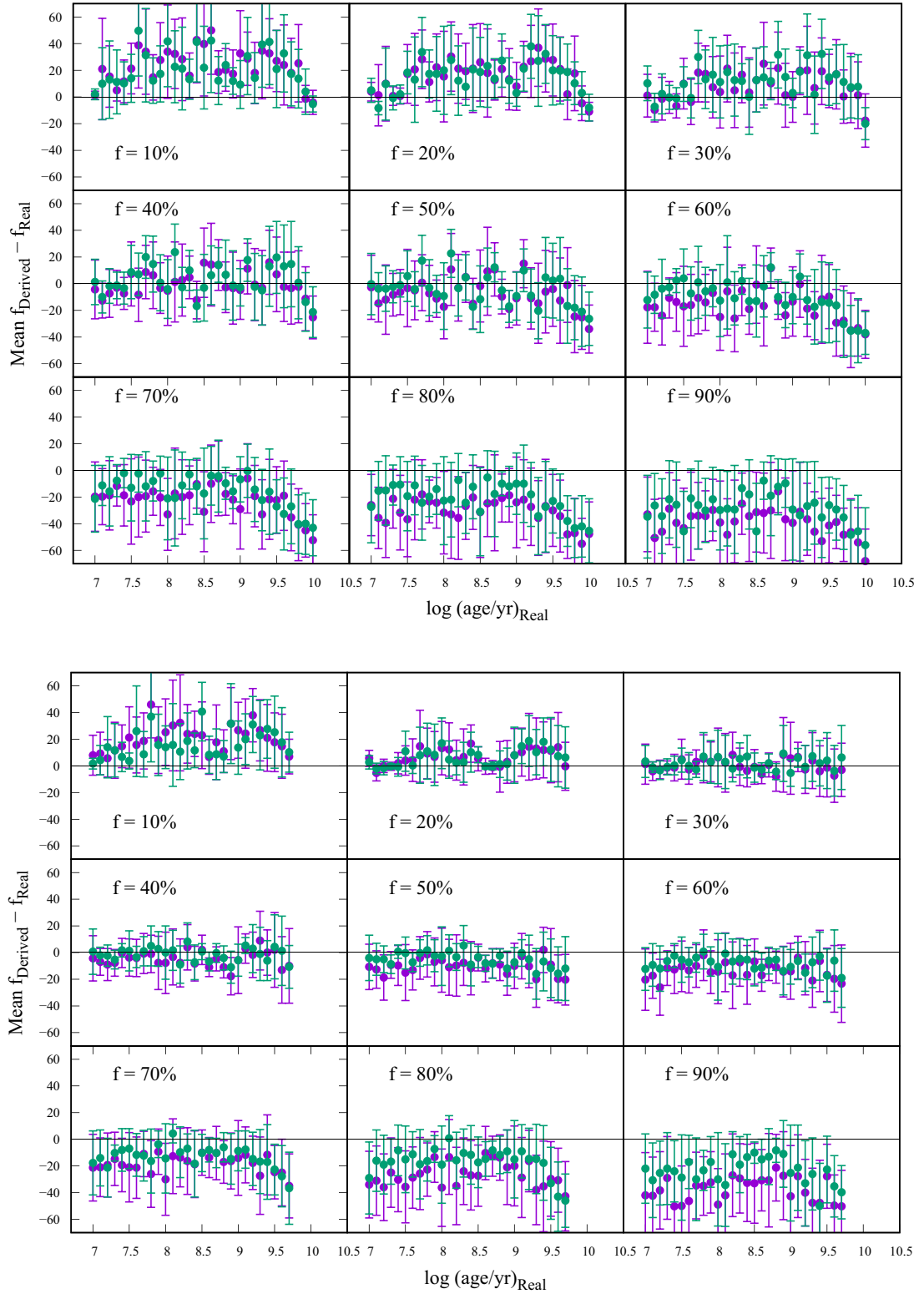


**Figure 9.** The mean of the derived mass fraction as a function of the input age. The top panel shows the results from  $\Delta \text{SSP} = 0.2$  and the lower panel shows the results from  $\Delta(\log(\text{age}/\text{yr})) = 0.5$ . The green dots represent results for  $S/N = 100$  and the purple dots represent the results for  $S/N = 50$ .

(D) The success rate (defined as the number of times the derived parameter matches the input parameter  $\pm 0.1$  dex) peaks around  $\log(\text{age/yr}) = 7.2$  and  $9.0$  and drops around  $8.6$  and  $> 9.5$  due to the similarity of SED shapes for those ages.

(E) Increasing the age gap in the mock clusters improves the derived parameters. However,  $\text{Age}(\text{SSP}_2)$  is still overestimated for  $\text{Age}(\text{SSP}_2) < 8.5$ .

(F) The derived mass fraction is overestimated for low mass fraction values and underestimated for high mass fraction values despite the age gap size. The best results are derived when the mass fraction is around 50 per cent.

## ACKNOWLEDGEMENTS

RA thanks the Space Telescope Science Institute for a sabbatical visitorship including travel and subsistence support as well as access to their science cluster computer facilities. The initial analysis of this work was done using the Geospatial Analysis Center (GAC) computers at the American University of Sharjah. We acknowledge the support of GAC and IT staff. This work is based on work supported in part by the FRG17-R-06 and EFRG-18-SET-CAS-74 grants P.I., R. Asa'd from American University of Sharjah as well as Mohammed Bin Rashid Space Center (MBRSC) grant 201602.SS.AUS P.I. Randa Asa'd at the American University of Sharjah.

## DATA AVAILABILITY

The model spectra of all mock star clusters and SSP models created for this paper are available through CDS.

## REFERENCES

- Ahumada A. V., Claria J. J., Bica E., Dutra C. M., 2002, *A&A*, 393, 855  
 Asa'd R. S., 2014, *MNRAS*, 445, 1679  
 Asa'd R., Goudfrooij P., 2020, *MNRAS*, 498, 2814 (Paper I)  
 Asa'd R. S., Hanson M. M., Ahumada A. V., 2013, *PASP*, 125, 1304  
 Asa'd R. S., Vazdekis A., Zeinelabdin S., 2016, *MNRAS*, 457, 2151  
 Asa'd R. et al., 2020, *ApJ*, 900, 138  
 Bastian N., de Mink S. E., 2009, *MNRAS*, 398, L11  
 Bastian N., Lardo C., 2018, *ARA&A*, 56, 83  
 Bastian N., Kamann S., Cabrera-Ziri I., Georgy C., Ekström S., Charbonnel C., de Juan Ovelar M., Usher C., 2018, *MNRAS*, 480, 3739  
 Bertelli G., Nasi E., Girardi L., Chiosi C., Zoccali M., Gallart C., 2003, *AJ*, 125, 770

- Cabrera-Ziri I. et al., 2020, *MNRAS*, 495, 375  
 Chilingarian I. V., Asa'd R., 2018, *ApJ*, 858, 63  
 Choi J., Conroy C., Byler N., 2017, *ApJ*, 838, 159  
 Cid Fernandes R., Gonzalez Delgado R. M., 2010, *MNRAS*, 403, 780  
 Conroy C., Gunn J. E., 2010, *ApJ*, 712, 833  
 Conroy C., Gunn J. E., White M., 2009, *ApJ*, 699, 486  
 Cordoni G., Milone A. P., Marino A. F., Di Criscienzo M., D'Antona F., Dotter A., Lagioia E. P., Tailo M., 2018, *ApJ*, 869, 139  
 Costa G., Girardi L., Bressan A., Chen Y., Goudfrooij P., Marigo P., Rodrigues T. S., Lanza A., 2019, *A&A*, 631, A128  
 Dupree A. K. et al., 2017, *ApJ*, 846, L1  
 Falcón-Barroso J., Sánchez-Blázquez P., Vazdekis A., Ricciardelli E., Cardiel N., Cenarro A. J., Gorgas J., Peletier R. F., 2011, *A&A*, 532, A95  
 Foreman-Mackey D., Sick J., Johnson B., 2014, python-fsps: Python bindings to fsps (v0.1.1). Available at: <https://doi.org/10.5281/zenodo.12157>  
 Gossage S. et al., 2019, *ApJ*, 887, 199  
 Goudfrooij P., Asa'd R. S., 2021, *MNRAS*, 501, 440 (Paper II)  
 Goudfrooij P., Puzia T. H., Kozhurina-Platais V., Chandar R., 2009, *AJ*, 137, 4988  
 Goudfrooij P., Girardi L., Correnti M., 2017, *ApJ*, 846, 22  
 Goudfrooij P., Girardi L., Bellini A., Bressan A., Correnti M., Costa G., 2018, *ApJ*, 864, L3  
 Kroupa P., 2001, *MNRAS*, 322, 231  
 Li C., Wang Y., Tang B., Milone A. P., Yang Y., Ji X., 2020, *ApJ*, 893, 17  
 Mackey A. D., Broby Nielsen P., 2007, *MNRAS*, 379, 151  
 Marino A. F., Przybilla N., Milone A. P., Da Costa G., D'Antona F., Dotter A., Dupree A., 2018, *AJ*, 156, 116  
 Martocchia S. et al., 2018, *MNRAS*, 477, 4696  
 Milone A. P., Bedin L. R., Piotto G., Anderson J., 2009, *A&A*, 497, 755  
 Palma T., Ahumada A., Claria J., Bica E., 2008, *Astron. Nachr.*, 329, 392  
 Puzia T. H., Kissler-Patig M., Thomas D., Maraston C., Saglia R. P., Bender R., Goudfrooij P., Hempel M., 2005, *A&A*, 439, 997  
 Puzia T. H., Kissler-Patig M., Goudfrooij P., 2006, *ApJ*, 648, 383  
 Sánchez-Blázquez P. et al., 2006, *MNRAS*, 371, 703  
 Santos J. F. C., Claria J. J., Ahumada A. V., Bica E., Piatti A. E., Parisi M. C., 2006, *A&A*, 448, 1023  
 Sun W., de Grijs R., Deng L., Albrow M. D., 2019, *ApJ*, 876, 113  
 Talavera M., Ahumada A., Santos J., Clariá J., Bica E., Parisi M., Torres M., 2010, *Astron. Nachr.*, 331, 323  
 Vazdekis A., Sánchez-Blázquez P., Falcón-Barroso J., Cenarro A. J., Beasley M. A., Cardiel N., Gorgas J., Peletier R. F., 2010, *MNRAS*, 404, 1639  
 Vazdekis A., Koleva M., Ricciardelli E., Röck B., Falcón-Barroso J., 2016, *MNRAS*, 463, 3409

This paper has been typeset from a  $\text{\TeX}/\text{\LaTeX}$  file prepared by the author.